1

Numerical Simulation in Steady flow of Non-Newtonian Fluids in Pipes with Circular Cross-Section

F.J. Galindo-Rosales[1] and F.J. Rubio-Hernández[2]
[1]*Transport Phenomena Research Center*
University of Porto, 4200-465 Porto
[2]*Department of Applied Physics II*
University of Málaga, 29071 Málaga
[1]*Portugal*
[2]*Spain*

1. Introduction

In the chemical and process industries, it is often required to pump fluids over long distances from storage to various processing units and/or from one plant site to another. There may be a substantial frictional pressure loss in both the pipe line and in the individual units themselves. It is thus often necessary to consider the problems of calculating the power requirements for pumping through a given pipe network, the selection of optimum pipe diameter, measurement and control of flow rate, etc. A knowledge of these factors also facilitates the optimal design and layout of flow networks which may represent a significant part of the total plant cost (Chhabra & Richardson, 2008).

The treatment in this chapter is restricted to the laminar, steady, incompressible fully developed flow of a non-Newtonian fluid in a circular tube of constant radius. This kind of flow is dominated by shear viscosity. Then, despite the fact that the fluid may have time-dependent behavior, experience has shown that the shear rate dependence of the viscosity is the most significant factor, and the fluid can be treated as a purely viscous or time-independent fluid for which the viscosity model describing the flow curve is given by the Generalized Newtonian model. Time-dependent effects only begin to manifest themselves for flow in non-circular conduits in the form of secondary flows and/or in pipe fittings due to sudden changes in the cross-sectional area available for flow thereby leading to acceleration/deceleration of a fluid element. Even in these circumstances, it is often possible to develop predictive expressions purely in terms of steady-shear viscous properties (Chhabra & Richardson, 1999).

The kind of flow considered in this chapter has been already studied experimentally by Hagen Poiseuille in the first half of the XIX Century for Newtonian fluids and it has analytical solution. However, even though in steady state non-Newtonian fluids can be treated as purely viscous, the shear dependence of viscosity may result in differential equations too complex to permit analytical solutions and, consequently, it is needed to use numerical techniques to obtain numerical solutions. It is in this context when Computational Rheology plays its role

(Crochet et al., 1985). Existing techniques for solving Newtonian fluid mechanics problems have often been adapted with ease to meet the new challenge of a shear-dependent viscosity, the application of numerical techniques being especially helpful and efficacious in this regards (Tanner & Walters, 1998).
Most of the text books dealing with the problem of non-Newtonian fluids through pipes, with a few exceptions, put emphasis on the solution for the power-law fluids, while there are many other industrially important shear-dependent behaviors that are left out of consideration. Here it is intendeded to cover this gap with the help of numerical techniques.

2. Flow problems

In this section we will introduce physical laws governing the deformation of matter, known as *conservation equations* or *field equations*, which are general for any kind of material. After this we will introduce the *constitutive equations*, which provide the viscosity (η) and the thermal conductivity (k) as a function of the state. Moreover, in order to close the entire system of equations, we have to define the thermodynamic relationships between the state variables, which are intrinsic of the material considered in the problem of the fluid. Clearly, these relationships depend on the kind of fluid being considered. Then, the boundary and initial conditions are presented as the equations needed to particularize the flow problem and complete the set of equations in order to be resolved, analytical or numerically. All these equations are defined as a stepping-off point for the study of steady flow of non-Newtonian fluids in pipes with circular cross-section.

2.1 Governing equations

The term *fluid dynamics* stands for the investigation of the interactive motion of a large number of individual particles (molecules or atoms). That means, the density of the fluid is considered high enough to be approximated as a continuum. It implies that even an infinitesimally small (in the sense of differential calculus) element of the fluid still contains a sufficient number of particles, for which we can specify mean velocity and mean kinetic energy. In this way, we are able to define velocity, pressure, temperature, density and other important quantities at each point of the fluid.
The derivation of the principal equations of fluid dynamics is based on the fact that the dynamical behaviour of a fluid is determined by the following conservation laws, namely:

1. the conservation of mass[1],
2. the conservation of momentum, and
3. the conservation of energy.

Hereafter, this set of equations will be known as the *field equations*. We have to supply two additional equations, which have to be thermodynamic relations between the state variables, like for example the pressure as a function of density and temperature, and the internal energy or the enthalpy as a function of pressure and temperature. Beyond this, we have to provide the viscosity (η) and the thermal conductivity (k) as a function of the state of the fluid, in order to

[1] In most of the processes ocurring in chemical engineering, fluids are generally compossed of different components and their concentrations might vary temporarily and spatially due to either potential chemical reactions or molecular difussion, therefore it would be necessary to consider the conservation of mass for each component being present in the fluid. However, we will consider in this chapter that fluids are sufficiently homogeneous and no chemical reactions occur in it. Then, the conservation of mass can be applied to the fluid as it was composed of only one component.

close the entire system of equations. Clearly, these relationships depend on the kind of fluid being considered (Blazek, 2001), and therefore they will be known hereafter as *constitutive equations*. Then, it can be summarized as **the governing equations consist of field equations and constitutive equations**.

In the isothermal theory, the conservation of energy equation is decoupled from the conservations of mass and momentum. Therefore, the field equations are reduced to the equation of continuity (Equation 1), which is a formal mathematical expression of the principle of conservation of mass, and the stress equations of motion, which arise from the application of Newton's second law of motion to a moving continuum (or the principle of balance of linear momentum) and the local expression of the principle of balance of angular momentum (Equation 2).

$$\frac{\partial \rho}{\partial t} + \nabla \cdot (\rho \vec{v}) \tag{1}$$

$$\frac{\partial \rho \vec{v}}{\partial t} + \nabla \cdot (\rho \vec{v} \vec{v}) = \nabla \cdot \overline{\overline{\tau}} + \rho \vec{f_m} \tag{2}$$

Consequently, the thermal conductivity coefficient and the thermodynamic relations between the state variables are not needed to be known, because they will not participate in the solution of isothermal problems. For this reason, they will not be considered in the rest of the chapter, since we will focus in isothermal problems, without external sources of energy. However, we still require of a relationship between the stress tensor and the suitable kinematic variables expressing the motion of the continuum, i.e. we require of a rheological equation of state.

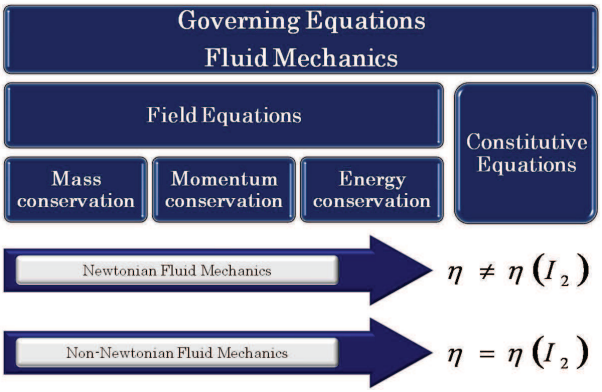

Fig. 1. The governing equations consist of field equations (conservations of mass, momentum and energy) and constitutive equations. The constitutive equations distinguish classical fluid mechanics from non-Newtonian fluid mechanics, due to Newton's viscosity law is valid for all flow situations (the viscosity is constant at any shear rate) and all Newtonian viscous fluids, but not for non-Newtonian fluids, for which their viscosities depend on the flow conditions (I_2 is the second invariant of the tensor of shear rates) among other parameters.

Independently on whether the problem is isothermal or not, the viscosity relates the stress to the motion of the continuum. This equation for non-Newtonian fluids is also known as rheological equation of state. Whereas the field equations are the same for all materials, constitutive equation will in general vary from one non-Newtonian material to another,

and possibly from one type of flow to another. It is this last point which distinguishes non-Newtonian fluid mechanics from classical fluid mechanics, where the use of Newton's viscosity law gives rise to the Navier-Stokes equations, which are valid for all Newtonian viscous fluids (Crochet et al., 1985). Figure 1 shows a sketch of the governing equations.
Finally, it will be also needed to define initial and boundary conditions in order to solve the specific problems.

2.1.1 Field equations for steady flow in pipes with circular cross-section

Independently on the constitutive equation, the stress tensor ($\overline{\overline{\tau}}$) can be assumed as the sum of hydrostatic pressure, corresponding to a static state of the fluid ($-p\overline{\overline{I}}$), and the viscous stresses ($\overline{\overline{\tau'}}$), which represent the dynamic part of the stress tensor. In 1845, Stokes deduced a constitutive viscosity equation (Equation 3) generalizing Newton's idea, which is valid for many fluids, known as Newtonian fluids:

$$\overline{\overline{\tau'}} = \overline{\overline{\overline{A}}} : \overline{\overline{\dot{\gamma}}}, \tag{3}$$

where $\overline{\overline{\overline{A}}}$ is a forth order tensor generally depending on time, position and velocity, and $\overline{\overline{\dot{\gamma}}}$ the deformation rate tensor[2]. For newtonian fluids, $\overline{\overline{\overline{A}}}$ does not depend on velocity. Those fluids not accomplishing the Equation 3 are known as Non-Newtonian Fluids.
In the particular case of having an isotropic fluid, the Equation 3 simplifies considerably in Equation 4

$$\overline{\overline{\tau'}} = 2\eta \left[\frac{1}{2} \left(\nabla\vec{v} + \nabla\vec{v}^T \right) - \frac{1}{3} \nabla \cdot \vec{v} \overline{\overline{I}} \right] + \eta_v \nabla \cdot \vec{v} \overline{\overline{I}}, \tag{4}$$

where η is the viscosity associated to the pure shear deformation of the fluid, and η_v is the volumetric viscosity coefficient and it is related to the volumetric deformation of the fluid due to normal forces. Then, for an isotropic fluid, the Navier-Stokes equation is obtained by introducing the Equation 4 in the Equation 2.

$$\frac{\partial \rho \vec{v}}{\partial t} + \nabla \cdot (\rho \vec{v} \vec{v}) = -\nabla p + \nabla \cdot \left[\eta \left(\nabla\vec{v} + \nabla\vec{v}^T \right) \right] + \nabla \left[\left(\eta_v - \frac{2}{3}\eta \right) \nabla \cdot \vec{v} \right] + \rho \vec{f_m}. \tag{5}$$

Moreover, if the fluid can be considered incompressible ($\rho = cte$), the equation of continuity reduces to Equation 6

$$\nabla \cdot \vec{v} = 0, \tag{6}$$

and, consequently, the Equation 5 simplifies reaching the form given by Equation 7

$$\rho \left(\frac{\partial \vec{v}}{\partial t} + \vec{v} \cdot \nabla\vec{v} \right) = -\nabla p + \nabla \cdot \left[\eta \left(\nabla\vec{v} + \nabla\vec{v}^T \right) \right] + \rho \vec{f_m}. \tag{7}$$

Reached this point, it is worth to point out that these reduced expressions of field equations (Equations 6 and 7) are only valid for an isotropic and incompressible fluid in isothermal conditions. It is now the moment of considering the simplifications of the field equations due to the facts that the fluid is flowing here in laminar steady state through an horizontal cross-section pipe (Figure 2).

[2] Also known as the rate-of-strain tensor: $\overline{\overline{\dot{\gamma}}} = \nabla\vec{v} + \nabla\vec{v}^T$.

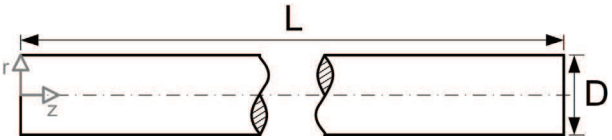

Fig. 2. Skecth of a pipe with lenght L and diameter $D << L$. The coordinates system here considered is cylindrical and its origin is placed and centered at the entrance of the pipe.

This is a canonical problem in Fluid Mechanics. The unidirectional and steady flow of a fluid through this pipe is originated by a constant gradient of reduced pressure $p_l = -\frac{\partial(p+\rho U)}{\partial z} = cte$, where U is a potential from which all massive forces derivate ($\vec{f_m} = -\nabla U$) and z is the axial coordinate. It can be proved that the laminar and fully developed flow in a pipe is axysymmetric, i.e. there are not dependences with the azimuthal coordinate ($\vec{e_\theta}$). Moreover, the r-component of vector $\vec{v}$ is zero. From the continuity equation (Equation 6), it can be derived that $\frac{dv_z}{dz} = 0$ and, consequently, the velocity vector expressed in cylindrical coordinates is given by Equation 8

$$\vec{v} = (v_r, v_\theta, v_z) = v_z \vec{e_z}, \tag{8}$$

with $v_z = v_z(r)$[3] Then, the deformation rate tensor is given by Equation 9

$$\nabla\vec{v} + \nabla\vec{v}^T = \begin{pmatrix} 0 & 0 & \frac{dv_z}{dr} \\ 0 & 0 & 0 \\ \frac{dv_z}{dr} & 0 & 0 \end{pmatrix}, \tag{9}$$

and, subsequently, the term $\nabla \cdot \left[\eta\left(\nabla\vec{v} + \nabla\vec{v}^T\right)\right]$ in Equation 7 is reduced to the expression given by Equation 10

$$\nabla \cdot \left[\eta\left(\nabla\vec{v} + \nabla\vec{v}^T\right)\right] = \begin{pmatrix} 0 \\ 0 \\ \frac{1}{r}\frac{d}{dr}\left(r\eta\frac{dv_z}{dr}\right) \end{pmatrix}. \tag{10}$$

In this way, the field equations are reduced to a second order ordinary differential equation (Equation 11) (Landau & Lifshitz, 1987). It must be noticed that this equation is needed to be completed with two boundary conditions and a constitutive equation, but not initial condition because the flow is steady.

$$p_l + \frac{1}{r}\frac{d}{dr}\left(r\eta\frac{dv_z}{dr}\right) = 0 \tag{11}$$

[3]This dependence can be deduced from the fact that, while v_z is zero at $r = D/2$ by the no-slip condition, in other r-value is that sure v_z is non-zero.

2.1.2 Boundary conditions

For a Newtonian fluid, the constitutive equation for the viscosity does not depend on the flow conditions and it is simply a constant coefficient $\eta = cte$. Therefore, the Equation 11 is linear and its general solution is given by Equation 12, where the values of the constants C_1 and C_2 will depend on the boundary conditions.

$$v_z(r) = -\frac{p_l r^2}{4\eta} + C_1 lnr + C_2 \tag{12}$$

Classically, in Fluid Mechanics, these boundary conditions consists of the following ones:

– The **no-slip condition** holds that the particles of fluid adjacent to the wall of the pipe move with the wall velocity (Equation 13)

$$v_z(r = D/2) = 0. \tag{13}$$

– The **no-singularity condition** consists of assuming that v_z is a continuous function and its first derivative exists and is also continuous, therefore the Equation 14 must be accomplished

$$\frac{dv_z}{dr}(r = 0) = 0. \tag{14}$$

Then, the Equation 12 reduces to Equation 15, i.e. the velocity profile for a Newtonian, isotropic and incompressible fluid under laminar and steady flow through a circular cross-section pipe is parabolic, as studied experimentally by Hagen in 1839 and Poiseuille in 1840 (Papanastasiou et al., 2000).

$$v_z(r) = \frac{p_l}{4\eta}\left(\frac{D^2}{4} - r^2\right) \tag{15}$$

However, when it is considered the laminar steady flow of a non-Newtonian fluid through this kind of pipes things change. Even though the no-singularity boundary condition still holds, the assumption of the no-slip condition is not as straightforward as it might seem. Rheologists have, for good reasons, been more concerned about the validity of the concept than workers in Newtonian fluid mechanics. With the benefit of decades of both theoretical and experimental interest, it is possible to assess that at least three factors are of importance concerning slip (Tanner & Walters, 1998):

– No effective slip can occur when molecular size is smaller than the wall roughness scale.

– For large molecules, relative to the wall roughness scale, the temperature and chemical adherence properties may be of great significance in setting the critical shear stress at which slip occurs.

– Normal pressure may assist in reducing slip.

Taking these factors about the slip at the wall into account, we will however assume that the no-slip boundary condition holds in all the cases here considered.

2.1.3 Constitutive equations for non-newtonian fluids

Constitutive equations (or rheological equations of state) are equations relating suitably defined stress and deformation variables (Barnes et al., 1993). The simplest example is the constitutive law for the Newtonian viscous liquid (Equation16), where a constant viscosity coefficient is sufficient to determine the behaviour of incompressible Newtonian liquids under any conditions of motion and stress. The measurement of this viscosity coefficient involves the use of a *viscometer*, defined simply as *an instrument for the measurement of viscosity*.

$$\overline{\overline{\tau'}} = \eta \overline{\overline{\dot{\gamma}}} \tag{16}$$

However, as the viscosity of non-Newtonian liquids may be dependent on the flow conditions, i.e. the rate-of-strain tensor, the viscometer is therefore inadequate to characterize the behaviour of these materials and has to be replaced by a *rheometer*, defined as *an instrument for measuring rheological properties*. One of the objectives of Rheometry is to assist in the construction of rheological equations of state (Walters, 1975).

If non-Newtonian viscosity, a scalar, is dependent on the rate-of-strain tensor, then it must depend only on those particular combination of components of the tensor that are not dependent on the coordinate system, the invariants of the tensor (Bird et al., 1987):

- $I_1 = \sum_{i=1}^{3} \dot{\gamma}_{ii}$.
- $I_2 = \sum_{i=1}^{3} \sum_{j=1}^{3} \dot{\gamma}_{ij} \dot{\gamma}_{ji}$.
- $I_3 = \sum_{i=1}^{3} \sum_{j=1}^{3} \sum_{k=1}^{3} \dot{\gamma}_{ij} \dot{\gamma}_{jk} \dot{\gamma}_{ki}$.

It can be deduced with ease that $I_1 = 0$ for an incompressible fluid. In addition, I_3 turns out to be zero for shearing flows. Hence, for the flow problems here considered, η is solely dependent on I_2. Actually, it is preferred to use $\dot{\gamma}$, the magnitude of the rate-of-strain tensor ($\overline{\overline{\dot{\gamma}}}$), instead of I_2, being both parameters related by the Equation 17 (Macosko, 1994)

$$\dot{\gamma} = \sqrt{\frac{1}{2} \sum_{i=1}^{3} \sum_{j=1}^{3} \dot{\gamma}_{ij} \dot{\gamma}_{ji}} = \sqrt{\frac{1}{2} I_2}. \tag{17}$$

As this chapter is devoted to the steady flow of non-Newtonian fluids in pipes with circular cross-section, which is a kind of flow dominated by shear viscosity and where the elasticity of the fluid has no considerable repercussions, the most suitable constitutive equation is given by the Generalized Newtonian Model (GNM) given by Equation 18. This is an inelastic model for which the extra stress tensor is proportional to the strain rate tensor, but the "constant" of proportionality (the viscosity) is allowed to depend on the strain rate. The inelastic model possesses neither memory nor elasticity, and therefore it is unsuitable for transient flows, or flows that calls for elastic effects (Phan-Thien, 2002).

$$\overline{\overline{\tau'}} = \eta(\dot{\gamma}) \overline{\overline{\dot{\gamma}}} \tag{18}$$

Consequently, Equation 11 can be rewritten for non-Newtonian liquids as Equation 19

$$p_l + \frac{1}{r} \frac{d}{dr} \left(r \eta(\dot{\gamma}) \frac{dv_z}{dr} \right) = 0. \tag{19}$$

The GNM is quite general because the functional form of $\eta(\dot{\gamma})$ is not specified. It must be given or fit the data to predict the flow properties. We will introduce different models for

$\eta(\dot{\gamma})$, but many other functional forms can be used and these can be found in the literature or in flow simulation softwares. Before that, it is important to keep in mind the main limitations of the GNM (Morrison, 2001):

- They rely on the modeling shear viscosity to incorporate non-Newtonian effects, and therefore it is not clear whether these models will be useful in nonshearing conditions.
- They do not predict shear normal stresses N_1 and N_2, which are elastic effects, and therefore they can not consider memory effects.

Nevertheless, the GNM enjoys success in predicting pressure-drop versus flow curves for steady flow of non-Newtonian fluids in pipes with circular cross-section.
As it has been mentioned above, it is possible to obtain $\eta(\dot{\gamma})$ by means of experiments carried out in a rheometer. In a shear rheometer, the material is undergone to simple shear conditions, for which the rate-of-strain tensor is given by the Equation 20

$$\overline{\overline{\dot{\gamma}}} = \left(\nabla\vec{v} + \nabla\vec{v}^T\right) \cong \begin{pmatrix} 0 & 0 & 0 \\ 0 & 0 & \frac{dv_\theta}{dz} \\ 0 & \frac{dv_\theta}{dz} & 0 \end{pmatrix}, \tag{20}$$

whose invariants are the following ones:

- $I_1 = tr\left(\overline{\overline{\dot{\gamma}}}\right) = 0$
- $I_2 = 2\left(\frac{dv_\theta}{dz}\right)^2$
- $I_3 = det\left(\overline{\overline{\dot{\gamma}}}\right) = 0$

In the case of a steady flow in pipes with circular cross-section, the rate-of-strain tensor is given by the Equation 9 and its invariants are the following ones:

- $I_1 = tr\left(\overline{\overline{\dot{\gamma}}}\right) = 0$
- $I_2 = 2\left(\frac{dv_z}{dr}\right)^2$
- $I_3 = det\left(\overline{\overline{\dot{\gamma}}}\right) = 0$

It can be observed that in both flow conditions the fluid is undergone to simple shear and it can be stated that $\dot{\gamma} = \sqrt{\frac{|I_2|}{2}} = |\frac{dv_\theta}{dz}| = |\frac{dv_z}{dr}|$. Then, the shear dependence of the viscosity in steady state observed in the rheological experiments could be used directly in Equation 19. It has been already probed that the experimental data obtained with a rheometer can be used successfully for the prediction of the transport characteristic in pipelines (Masalova et al., 2003).

2.1.3.1 GNM for shear thinning fluids

Most of non-Newtonian fluids (foods, biofluids, personal care products and polymers) undergone to steady shear exhibit shear thinnning behavior, i.e. their viscosity decreases with increasing shear rates. During flow, these materials may exhibit three distinct regions (see Figure 3): a lower Newtonian region where the apparent viscosity (η_0), usually called the limiting viscosity at zero shear rate, is constant with changing shear rates; a middle region where the apparent viscosity is decreasing with shear rate and the power law equation is

a suitable model for this region; and an upper Newtonian region where the viscosity (η_∞), called the limiting viscosity at infinite shear rate, is constant with changing shear rates (Steffe, 1996). Sometimes the position of the typical behaviour along the shear-rate axis is such that the particular measurement range used is either too low or too high to pick up the higher-shear-rate part of the curve[4].

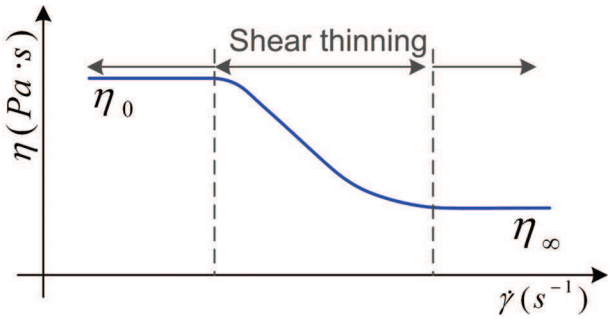

Fig. 3. Typical viscosity curve for a shear thinning behaviour containing the three regions: The two limiting Newtonian viscosities, η_0 and η_∞, separated by a shear thinning region.

One equation for $\eta(\dot{\gamma})$ that describes the whole shear thinning curve is called the Cross model, named after Malcolm Cross, a rheologist who worked on dye-stuff and pigment dispersions. He found that the viscosity of many suspensions could be described by the equation of the form given by Equation 21

$$\eta(\dot{\gamma}) = \eta_\infty + \frac{\eta_0 - \eta_\infty}{1 + (K\dot{\gamma})^m}, \tag{21}$$

where K has the dimensions of time, and m is dimensionless. The degree of shear thinning is dictated by the value of m, with m tending to zero describes more Newtonian liquids, while the most shear-thinning liquids have a value of m tending to unity. If we make various simplifying assumptions, it is not difficult to show that the Cross equation can be reduced to Sisko[5] or power-law models[6]. The Carreau model is very similar to the Cross model (Equation 22)

$$\eta(\dot{\gamma}) = \eta_\infty + \frac{\eta_0 - \eta_\infty}{\left[1 + (K\dot{\gamma})^2\right]^{m/2}}, \tag{22}$$

both (Cross and Carreau equations) are the same at very low and very high shear rates, and only differ slightly at $K\dot{\gamma} \approx 1$ (Barnes, 2000).
The use of Cross or Carreau models in the Equation 19 results in a differential equation that can not be solved analytically and, thefore, numerical techniques are needed.
It is worth to emphasize here that due to the boundary condition of no-singularity imposed at the axis of symmetry, it is highly important choosing a model which contains what happens to the viscosity at low shear rates in order to solve this problem.

[4]Note that the typical shear-rate range of most laboratory viscometers is between 10^{-2} and $10^3\ s^{-1}$

[5]When the viscosity is just coming out of the power-law region of the flow curve and flattening off towards η_∞, the Sisko model is the best fitting equation: $\eta(\dot{\gamma}) = \eta_\infty + k\dot{\gamma}^{n-1}$.

[6]In many situations, $\eta_0 >> \eta_\infty$, $K\dot{\gamma} >> 1$, and η_∞ is small. Then the Cross equation (with a simple change of the variables K and m) reduces to the well-known power-law (or Ostwald-de Waele) model, which is given by $\eta(\dot{\gamma}) = k\dot{\gamma}^{n-1}$, where k is called the consistency and n the power-law index.

2.1.3.2 GNM for shear thickening fluids

Shear thickening is defined in the British Standard Rheological Nomenclature as the increase of viscosity with increase in shear rate (Barnes, 1989). This increase in the effective viscosity occurs when the increasing shear rate exceeds a certain critical value. Although shear thickening fluids (STFs) are much less common than shear thinning materials in industry, an increasing number of applications take advantage of the shear thickening behaviour to improve their performance, i.e. the incorporation of STFs to Kevlar® fabrics in order to improve the ballistic protection (Lee et al., 2003; Kirkwood et al., 2004) and enhance stab resistance (Decker et al., 2007). However, shear thickening is an undesirable behaviour in many other cases and it should never be ignored, because this could lead to technical problems and even to the destruction of equipment, i.e. pumps or stirrers (Mezger, 2002).

Figure 4 shows the viscosity curve of a STF containing the three characteristic regions typically exhibited: slight shear thinning at low shear rates, followed by a sharp viscosity increase over a threshold shear rate value (critical shear rate), and a subsequent pronounced shear thinning region at high shear rates. Nowadays, the physics of the phenomenon is deeply understood thanks to the use of modern rheometers, scattering techniques, rheo-optical devices and Stokesian dynamic simulations (Bender & Wagner, 1996; Hoffman, 1974; Boersma et al., 1992; D'Haene et al., 1993; Hoffman, 1998; Maranzano & Wagner, 2002; Larson, 1999). However, there is a lack of experimental or theoretical models able to predict the whole effective viscosity curve of STFs, including the shear thinning behaviours normally present in these materials for low enough and high enough values of the shear rate.

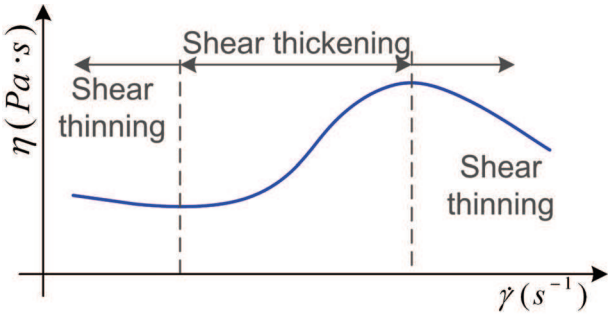

Fig. 4. Typical viscosity curve for a shear thickening behaviour containing the three regions: The two limiting shear thinning behaviours separated by a shear thickening region.

As it has been mentioned above, many functional forms have been proposed in the past for $\eta(\dot{\gamma})$ in the case of shear thinning fluids. In contrast, for shear thickening fluids only the power-law model, given by (Equation 23), has been commonly used

$$\eta(\dot{\gamma}) = k\dot{\gamma}^{n-1}. \tag{23}$$

Its major drawback is that power-law model can only fit the interval of shear rates where the viscosity increases with the shear rate $n > 1$, but it fails to describe the low and the high shear rate regions (Macosko, 1994), where shear-thinning behaviours are normally observed.

Very recently, Galindo-Rosales et al. (2010) have provided a viscosity function for shear thickening behavior able to cover these three characteristic regions of the general viscosity curve exhibited by STF. It consists in using a piecewise definition, taking the three different

regions into account separately. According to this approach, they have defined the viscosity function as follows,

$$\eta(\dot{\gamma}) = \begin{cases} \eta_I(\dot{\gamma}) & \text{for } \dot{\gamma} \leq \dot{\gamma}_c, \\ \eta_{II}(\dot{\gamma}) & \text{for } \dot{\gamma}_c < \dot{\gamma} \leq \dot{\gamma}_{max}, \\ \eta_{III}(\dot{\gamma}) & \text{for } \dot{\gamma}_{max} < \dot{\gamma}, \end{cases} \tag{24}$$

where $\eta_i(\dot{\gamma})$ is the viscosity function that fits the zone i of the general viscosity curve (for $i = I, II, III$). As it was pointed out by Souza-Mendes & Dutra (2004), the functions η_i must be chosen such that both, the composite function given by Equation 24, as well as its derivative with respect to $\dot{\gamma}$, are continuous. This procedure avoids practical problems in fitting procedures and in numerical simulations. The viscosity function proposed in the work of Galindo-Rosales et al. (2010), given by Equation 25, accomplishes these smoothness requirements.

$$\eta(\dot{\gamma}) = \begin{cases} \eta_I(\dot{\gamma}) = \eta_c + \frac{\eta_0 - \eta_c}{1 + \left[K_I\left(\frac{\dot{\gamma}^2}{\dot{\gamma} - \dot{\gamma}_c}\right)\right]^{n_I}} & \text{for } \dot{\gamma} \leq \dot{\gamma}_c, \\ \eta_{II}(\dot{\gamma}) = \eta_{max} + \frac{\eta_c - \eta_{max}}{1 + \left[K_{II}\left(\frac{\dot{\gamma} - \dot{\gamma}_c}{\dot{\gamma} - \dot{\gamma}_{max}}\right)\dot{\gamma}\right]^{n_{II}}} & \text{for } \dot{\gamma}_c < \dot{\gamma} \leq \dot{\gamma}_{max}, \\ \eta_{III}(\dot{\gamma}) = \frac{\eta_{max}}{1 + [K_{III}(\dot{\gamma} - \dot{\gamma}_{max})]^{n_{III}}} & \text{for } \dot{\gamma}_{max} < \dot{\gamma}. \end{cases} \tag{25}$$

It must be noticed that the parameters appearing in the branches of Equation 25 have the same dimensions and interpretation than those analogous for the Cross model (Equation 21): K_i (for $i = I, II, III$) possess dimension of time and are responsible for the transitions between the plateaus and the power-law, while the dimensionless exponents n_i are related to the slopes of the power-law regimes. Equation 25 is able to capture the three regimes characteristic of STF materials.

Then, substituting any the form of $\eta(\dot{\gamma})$ given in Equation 25 in the Equation 19 will results in a differential equation that can not be solved analytically and, thefore, numerical techniques will be needed again.

3. Numerical simulations

Classical Fluid Mechanics offers a wide variety of possibilities with regards to numerical algorithms based on finite elements, finite volume, finite differences and spectral methods (Wesseling, 2001). Computational rheologists do not have a recipe which lets them know which one is more suitable to work with in each particular problem, although most of the published works related to solve 2-D problems in steady state are based on finite element methods (Keunings, 1999). However, it has been proved that finite volume methods produce better results (O'Callaghan et al., 2003) due mainly to a good conservation of the fluid properties (mass, momentum and energy) and they allow to discretize complex computational domain in a simpler way (Fletcher, 2005).

The problem considered here, because of its geometrical features, can be solved by any of the numerical techniques already mentioned, although we have finally used the finite volume technique (Pinho & Oliveira, 2001; Pinho, 2001). As the flow problem is axysymmetric, the volume domain can be simplified to a 2-D domain with a length[7] ($L = 2$ m) and a width

[7] Its lenght is long enough to ensure that the regime of fully developed flow is reached.

($D = 1$ cm $<< L$). This domain is meshed by rectangles in a structured grid: in z-axis from the inlet (ratio 1.05 and 500 nodes) and r-axis from the axis (ratio 1.0125 and 50 nodes), which has been validated by correlating the analytical and numerical results given for the case of a Newtonian fluid (Figure 5).

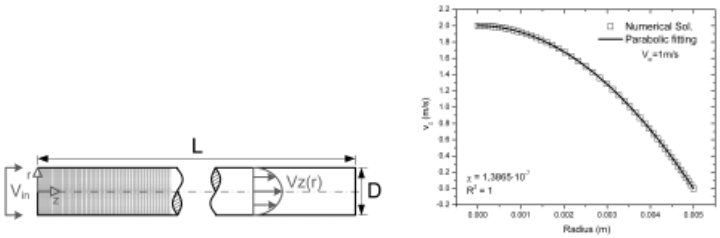

(a) (b)

Fig. 5. (a) Horizontal pipeline with $L >> R$ in order to ensure that the flow reaches the fully developed region. (b) Validation of the grid by means of the comparison between the numerical result and the analytical solution of the fully developed velocity profile for a Newtonian liquid.

As a consequence of the friction drag, there is a pressure drop. The energy required to compensate the dissipation due to frictional losses against the inside wall and to keep the fluid moving is usually supported by a pump. A large amount of data obtained experimentally for many different Newtonian fluids in pipes having diameters differing by orders of magnitude and roughness have been assembled into the so-called friction-factor chart or Moody chart, relating the friction factor with Reynolds number in laminar and turbulent regime and relative roughness. In laminar flow, the friction factor does not depend on the roughness of the inner surface of the pipe and can be calculated by the Equation 26

$$f = \frac{16}{Re}, \tag{26}$$

where f is the friction factor and Re is the Reynolds number. Nevertheless, when the fluid is non Newtonian, the Moody chart and the Equation 26 are useless due to in non-Newtonian fluids there is an extra dissipation of energy expent in modifying the internal structure of the fluid[8]. It then is needed to analyse the particular flow behaviour of the fluid considered, obtain its constitutive equation and solve the momentum conservation equation in order to characterize the steady flow in a pipe of circular cross-section.

As an example of how to proceed, two different non-Newtonian fluids (shear thinning and shear thickening fluids) are considered here. Firstly, their constitutive forms for $\eta(\dot{\gamma})$ will be obtained from their experimental viscosity curves. Secondly, the momentum conservation equation in the steady state (Equation 19), considering axysimmetry and a cylindrical coordinate system centered in the axis of the pipe, will be solved numerically by volume finite methods. In order to have shear rates values within the limits of the experimental results for each sample, the velocity inlet was always imposed at values below 0.1 m/s. Thus, the

[8] As it is oulined in the following subsection, the variations in the viscosity are due to variation in the internal order of the fluid, which is possible thanks to the mechanical energy suplied by the shearing motion.

velocity profile, shear rate, apparent viscosity, pressure drop and friction factor were obtained for each sample as function of velocity.

3.1 Experimental data set

Aerosil® fumed silica is a synthetic, amorphous and non-porous silicon dioxide produced by Degussa A.G (Degussa, 1998) following a high temperature process. Aerosil® 200 presents a highly hydrophilic surface chemistry with surface silanol groups ($Si-OH$) that can participate in hydrogen bonding. Because of the relatively high surface area ($200 m^2/g$) of these particles, the surface functional groups play a major role in the behavior of fumed silica Degussa (2005a). In the unmodified state, the silanol group imparts a hydrophilic character to the material. However, it is possible to modify its surface chemistry by means of a chemical after treatment with silane. In this way, Aerosil® R805 is obtained from Aerosil® 200 particles by replacing silanol groups with octadecylsilane chains, which results in an hydrophobic behaviour of the particles (Degussa, 2005b).

The degree of network formation by fumed silica in a liquid depends on the concentration of solid and type (hydrophilic versus hydrophobic) of silica, as well as the nature (polarity) of the suspending medium. Therefore, these three main factors allow to the suspensions of Aerosil® fumed silica inside a fluid possess a variety of rheological behaviors (Khan & Zoeller, 1993; Raghavan & Khan, 1995). This variety of rheological behaviors makes silica particle a very interesting filler from the point of view of a wide range of applications. For example, gels of fumed silica in mineral or silicone oils are used as filling compounds in fiber-optic cables, while in polyethylene glycols are being considered for application as polymer electrolytes in rechargeable lithium batteries(Jáuregui Beloqui & Martin Martinez, 1999; Dolz et al., 2000; Walls et al., 2000; Li et al., 2002; Fischer et al., 2006; Yziquel et al., 1999; Ouyang et al., 2006).

It has been already reported elsewhere (Galindo-Rosales & Rubio-Hernández, 2007; 2010) that suspensions of Aerosil® R805 and Aerosil® 200 in Polypropylene Glycol (PPG) with a molecular weight of 400 g/mol exhibit completely different rheological behaviour. PPG molecules interfere in the formation of the fumed silica network by attaching itself to the active $Si-OH$ sited on the silica surface. Therefore no bridging between silica particles occurs with polar solvents, such as polypropylene glycol, that have a stronger affinity for fumed silica than that existing between two fumed silica. The solvent attaches itself to the surface silanol group of the fumed silica rendering it inactive for further network formation. For that reason, when dispersing Aerosil® 200 in polypropylene glycol, it is expected that primary aggregates interconnect, originating flocs with different sizes depending on the weight fraction. On the contrary, a large interconnection between the flocs, which may result in a three dimensional structure, should not take place. Therefore, the suspension would be non-flocculated (Raghavan & Khan, 1997; Raghavan et al., 2000). However the presence of octadecylsilane chemical bonds on the surface of Aerosil® R805 avoids that PPG molecules attached to the silica particles and lets them develop a three dimensional network without interacting chemically with polypropylene gycol chains. So a flocculated suspension is formed (Khan & Zoeller, 1993).

The steady viscosity curves, shown in Figure 6, represent the steady viscosity reached by the suspensions at different values of shear rates. Therefore, the shape of these curves is a consequence of the order achieved by silica particles inside the polymer matrix under flow conditions. According to the previous analysis, Aerosil® R805 suspension is flocculated after a long time at rest, and the network breaks down when subjected to shear, a behavior known as shear thinning. Figure 6 confirms that the higher the shear rate applied, the lower the apparent

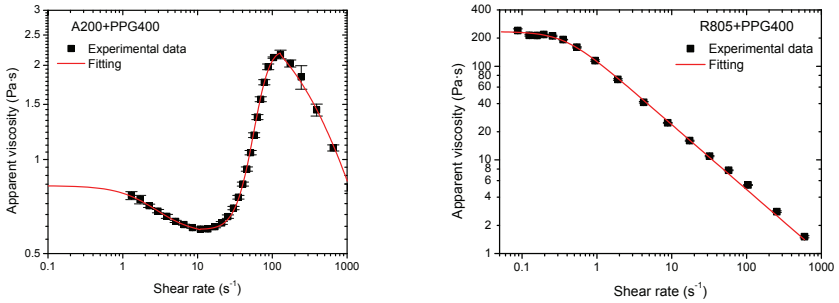

(a) (b)

Fig. 6. Steady viscosity curve of A200 (a) and R805 (b) suspension in PPG400 at 5 %v/v and 25 ^{o}C fitted by Equation 25 and Carreau model, respectively.

steady viscosity value. As the interconnection between flocs and aggregates disappear under the action of shear stress, the resistance to the flow decreases. On the other hand, the Aerosil® 200 suspension presents a flow curve in which three zones can be distinguished. At low shear rates, there is a reversible and slight shear thinning region ($\dot{\gamma} \leq 10.91 \pm 0.05 s^{-1}$). In the interval of shear rates between $10.91 \pm 0.05 s^{-1}$ and $129 \pm 4 s^{-1}$, the viscosity increases with the shear rate (shear thickening). Finally, at high shear rates ($\dot{\gamma} \geq 129 \pm 4 s^{-1}$), the viscosity decreases again in a more pronounced way. This shape of the flow curve is a consequence of the internal microstructure developed by the nanoparticles, and it is characteristic for non-flocculated suspensions, in agreement with the results and analysis presented above. At low shear rates the decrease in the viscosity is a consequence of the effect that the supplied mechanical energy has on the existing flocs. Under shear, agglomerates either break down into smaller sizes or stretch aligning in the flow direction. Both contribute to decrease the resistance to the flow and, subsequently, a viscosity descend. The higher the shear rate applied, the more prominent is this effect. However, when the shear rate is higher than a critical value $\dot{\gamma}_c$, the flocs are forced to connect to each other by hydrodynamic forces. This structure formation during flow results in an increase of the flow resistance and, therefore, leads to an increase of viscosity, as well as to the presence of the shear thickening region observed in Figure 6. However, this situation is metastable. When shear rate is higher than a maximum value ($\dot{\gamma}_m$), the stability of the structure developed under flow is lost and the structure breaks down, decreasing the viscosity (Vermant & Solomon, 2005). Shear thickening is not expected at such low volume fraction (Barnes, 1989). Actually, this fact can be explained only by taking into consideration the difference of aggregation between Euclidean and fractal solids. As consequence of their fractal nature, individual silica particles are linked forming open primary aggregates, leading to an effective dispersed phase volume ϕ_{eff} much larger than the nominal one, ϕ_s (Raghavan & Khan, 1997).

The equilibrium viscosity curves of the Aerosil® R805 suspension here considered, shown in Figure 6, can be fitted very accurately by Carreau Model, whose equation is given by Equation 22. This form of $\eta(\dot{\gamma})$ is able to predict the shape of the general flow curve for shear thinning behavior because of its four parameters (see Figure 6)[9].

[9]Non-linear least-squares regression method based on the Levenberg-Marquardt algorithm has been

Substituting Equation 22 in Equation 19, the differential equation which predicts the laminar, steady and fully developed velocity profile of our samples when they would flow through a duct is obtained (Equation 27)

$$p_l + \frac{1}{r}\frac{d}{dr}\left[r\left(\eta_\infty + \frac{\eta_0 - \eta_\infty}{\left[1 + \left(K|\frac{dv_z}{dr}|\right)^2\right]^{m/2}} \right)\frac{dv_z}{dr} \right] = 0, \tag{27}$$

whose boundary conditions are the same exposed above.
The equilibrium viscosity curves of the Aerosil® 200 suspension is also shown in Figure 6 and it can be fitted very accurately by Equation 25. This form of $\eta(\dot{\gamma})$ is able to predict the shape of the general flow curve for shear thickening behavior because of its eleven parameters (see Figure 6).
Substituting Equation 25 in Equation 19, a set of three differential equations is obtained (Equations 28), which predicts the laminar, steady and fully developed velocity profile of the suspension of A200 in PPG 400 at 5 %v/v and 25 ^{o}C, not having any of them analytical solutions. In order to solve them, numerical methods are needed.

$$\begin{aligned}
&p_l + \tfrac{1}{r}\tfrac{d}{dr}\left[r\left(\eta_c + \frac{\eta_0 - \eta_c}{1+\left[K_I\left(\frac{|\frac{dv_z}{dr}|^2}{|\frac{dv_z}{dr}|-\dot{\gamma}_c}\right)\right]^{n_I}} \right)\frac{dv_z}{dr} \right] = 0 && \text{for } |\tfrac{dv_z}{dr}| \le \dot{\gamma}_c,\\
&p_l + \tfrac{1}{r}\tfrac{d}{dr}\left[r\left(\eta_{max} + \frac{\eta_c - \eta_{max}}{1+\left[K_{II}\left(\frac{|\frac{dv_z}{dr}|-\dot{\gamma}_c}{|\frac{dv_z}{dr}|-\dot{\gamma}_{max}}\right)|\tfrac{dv_z}{dr}|\right]^{n_{II}}} \right)\frac{dv_z}{dr} \right] = 0 && \text{for } \dot{\gamma}_c < |\tfrac{dv_z}{dr}| \le \dot{\gamma}_{max},\\
&p_l + \tfrac{1}{r}\tfrac{d}{dr}\left[r\left(\frac{\eta_{max}}{1+\left[K_{III}\left(|\frac{dv_z}{dr}|-\dot{\gamma}_{max}\right)\right]^{n_{III}}} \right)\frac{dv_z}{dr} \right] = 0 && \text{for } \dot{\gamma}_{max} < |\tfrac{dv_z}{dr}|.
\end{aligned} \tag{28}$$

3.2 Results and discussion

Here are exhibited the results obtained from solving numerically the differential equations defined above.
Figure 7 shows the velocity profiles normalized by its maximum value, which is reached at the axis of symmetry (at $r = 0$), for the suspensions of A200 and R805 in PPG400 at 5 %v/v and 25 ^{o}C. It can be observed that both do not follow a parabolic profile, as it would be the Newtonian case. In spite of this, their velocity profiles depend on the velocity impose at the inlet of the pipe.
Different velocity profiles imply different shear rates across the section of the pipe, varying from zero at the axis of symmetry to its highest value at the neighborhood of the wall. In addition, the shear rates are higher for higher values of the inlet velocity, as it is shown in Figure 8.
It is noticeable that in the case of the A200, due to its shear thickening behavior, the viscosity increases with the velocity inlet and in the vicinity of the solid wall, where the shear rates are higher, in opposition what happen to R805 suspension. Around the axis, the shear conditions

used to fit the experimental data to the models here considered.

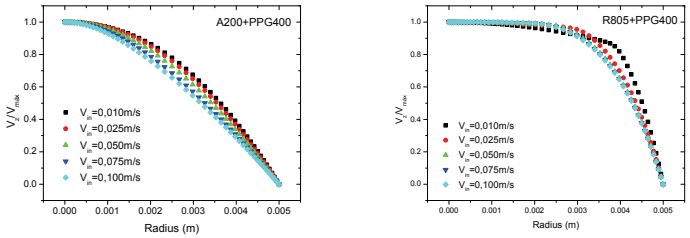

(a) (b)

Fig. 7. Velocity profiles normalized by its maximum value, which is reached at the axis of symmetry (at $r = 0$), for the suspensions of A200 (a) and R805 (b) in PPG400 at 5 %v/v and 25 ^{o}C.

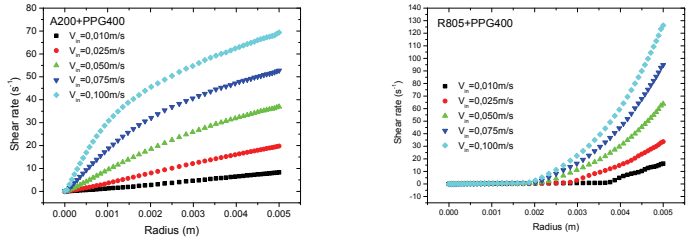

(a) (b)

Fig. 8. Shear rate evolution across the section of the pipe in the fully developed region for the suspensions of A200 (a) and R805 (b) in PPG400 at 5 %v/v and 25 ^{o}C.

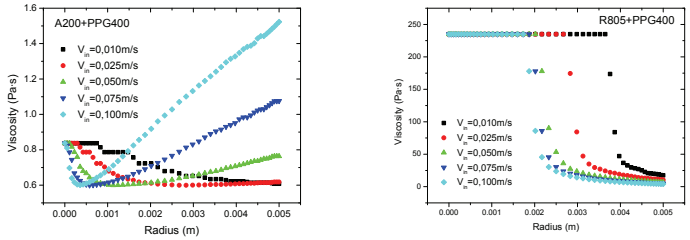

(a) (b)

Fig. 9. Variation of the steady viscosity across the section of the pipe in the fully developed region for the suspensions of A200 (a) and R805 (b) in PPG400 at 5 %v/v and 25 ^{o}C.

are almost null, what implies that in the A200 suspension the viscosity is relatively low, and relatively high for the R805, according to their viscosity curves (Figure 9). Therefore, that results in different shapes of the velocity profile, which is sharper for the shear thickening suspension and flatter for the one with shear thinning behavior (Figure 7).

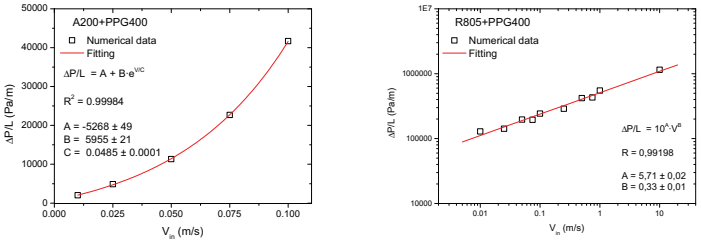

(a) (b)

Fig. 10. Pressure-drop per unit of length of the duct as a function of the velocity inlet. Results for the suspensions of A200 (a) and R805 (b) in PPG400 at 5 %v/v and 25 ^{o}C.

Non linear differences in the viscosity with the inlet velocity will result in differences in the pressure losses with regards to Hagen-Poiseuille solution. The pressure-drop per meter of pipe is shown in Figure 10 for different values of velocity inlet. It must be notice that the Reynolds number has not been used for those graphs, the reason is that this is a non-dimensional parameter useful when the viscosity is constant and here it is not the case. For a Newtonian flow, it is already known that pressure losses are proportional to the velocity inlet, however, in the case of non-Newtonian fluids, it would depend of their rheological behavior. In the case under study, the pressure-drop for a shear thickening behavior grows exponentially with the velocity inlet, while for the shear thinning one it does potentially. The values of losses are much higher for the case of R805 suspension, due to its higher viscosity values.

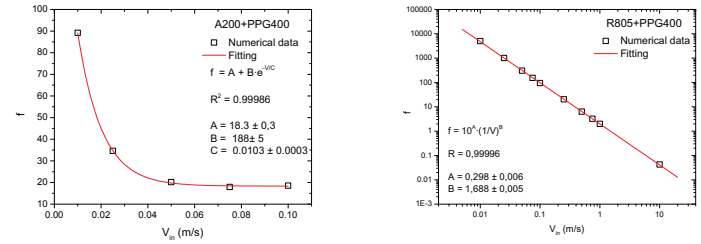

(a) (b)

Fig. 11. Friction factor as a function of the velocity inlet. Results for the suspensions of A200 (a) and R805 (b) in PPG400 at 5 %v/v and 25 ^{o}C.

This information can also be given expressed by the friction factor (Figure 11). It can be observed that the friction factor in the laminar regime does not depend inversely proportional to the velocity, but it follows a potential or exponential law, depending on the rheological properties of the fluid.

4. Other kind of flows

In this chapter we have been focused in the use of numerical techniques to solve the flow problem of laminar, steady and fully developed flow of non-Newtonian fluids, whose viscosity is described by the GNM. These constitutive equations do not consider elastic behavior and are perfect to describe this kind of flow due to it is dominated by viscous effects. Numerical techniques here are needed beacuse of non-linearities introduced by the constitutive equations of the fluids.

However, there are many other flow geometries in which elastic behaviors are relevant, i.e. contraction/expansion geometries, cross-slot, etc. Then, viscoelastic models must be used as constitutive equations for these fluids instead of the GNM. In this cases, because of complexities in the geometry and the constitutive equation, numerical techniques are also needed to obtain information about the flow properties. Those readers interested in this kind of flows are strongly recommended to have a look at the works of Prof. R. Keunings et al., Prof. K. Walters et al., Prof. M.J. Crochet et al. or Prof. F.T. Pinho et al., among others.

5. References

Barnes, H. A. (1989). Shear-thickening (dilatancy) in suspensions of nonaggregating solid particles dispersed in newtonian liquids, *Journal of Rheology* 32: 329–366.

Barnes, H. A. (2000). *Handbook of elementary rheology*, The university of Wales Institute of Non-Newtonian Fluid Mechanics, United Kingdom.

Barnes, H. A., Hutton, J. F. & Walters, K. (1993). *An introduction to Rheology*, Rheology Series, vol. 3, Ed. Elsevier Science Publishers B.V., Netherlands.

Bender, J. & Wagner, N. J. (1996). Reversible shear thickening in monodisperse and bidisperse colloidal dispersions, *Journal of Rheology* 40(5): 899–916.

Bird, R. B., Armstrong, R. C. & Hassager, O. (1987). *Dynamics of polymeric liquids. Volume 1 Fluid Mechanics*, John Wiley and Sons, Inc., USA.

Blazek, J. (2001). *Computational Fluid Dynamics: Principles and Applications*, Elsevier Science Ltd, Great Britain.

Boersma, W. H., Laven, J. & Stein, H. N. (1992). Viscoelastic properties of concentrated shear-thickening dispersions, *Journal of Colloid and Interface Science* 419(1): 10–22.

Chhabra, R. P. & Richardson, J. F. (1999). *Non-Newtonian flow in the process industries. Fundamentals and engineering applications*, Butterworth-Heinemann, USA.

Chhabra, R. P. & Richardson, J. F. (2008). *Non-Newtonian flow and applied rheology*, Butterworth-Heinemann, USA.

Crochet, M. J., Davies, A. R. & Walters, K. (1985). *Numerical simulation of non-Newtonian flow*, Rheology Series, vol. 1, Ed. Elsevier Science Publishers B.V., Netherlands.

Decker, M. J., Halbach, C. J., Nam, C. H., Wagner, N. J. & Wetzel, E. D. (2007). Stab resistance of shear thickening fluid (stf)-treated fabrics, *Composites Science and Technology* 67: 565–578.

Degussa, A. G. (1998). Basic characteristics of aerosil®, *Technical Bulletin - Pigment* 6.

Degussa, A. G. (2005a). Aerosil®200, hydrophilic fumed silica, *Product Information* .

Degussa, A. G. (2005b). Aerosil®R805, hydrophobic fumed silica, *Product Information* .

D'Haene, P., Mewis, J. & Fuller, G. G. (1993). Scattering dichroism measurements of flow-induced structure of a shear thickening suspension, *J. Colloid Interface Sci.* 156: 350–358.

Dolz, M., González, F., Delegido, J., Hernández, M. & Pellicer, J. (2000). A time-dependent

expression for thixotropic areas. application to aerosil 200 hydrogels, *Journal of Pharmaceutical Sciences* 89(6): 790–797.

Fischer, C., Braun, S. A., Bourban, P. E., Michaud, V., Plummer, C. J. G. & Manson, J. A. E. (2006). Dynamic properties of sandwich structures with integrated shear-thickening fluids, *Smart Materials and Structures* 15: 1467–1475.

Fletcher, C. A. J. (2005). *Computational Techniques for Fluid Dynamics. Volume 1-Fundamental and general techniques*, Ed. Springer Verlag, Berlin, Germany.

Galindo-Rosales, F. J. & Rubio-Hernández, F. J. (2007). Influence of the suspending phase on the rheological behaviour of aerosil R805 suspensions, *Annual Transactions of the Nordic Rheology Society*, Vol. 15, Juvenes Print, Tampere, Finland, pp. 73–79.

Galindo-Rosales, F. J. & Rubio-Hernández, F. J. (2010). Static and dynamic yield stresses of aerosil® 200 suspension in polypropylene glycol, *Applied Rheology* 20(2): 22787.

Galindo-Rosales, F.J., Rubio-Hernández, F.J. & Sevilla, A. (2010). An apparent viscosity function for shear thickening fluids (submitted to Journal of Non-Newtonian Fluid Mechanics).

Hoffman, R. L. (1974). Discontinuous and dilatant viscosity behavior in concentrated suspensions II: Theory and experimental tests, *J. Colloid Interface Sci.* 46(3): 491–506.

Hoffman, R. L. (1998). Explanations for the cause of shear thickening in concentrated colloidal suspensions, *Journal of Rheology* 42(1): 111–123.

Jaúregui-Beloqui, B., Fernández-García, J.C., Orgilés-Barceló, C.A., Mahiques-Bujandab, M.M. & Martín-Martínez, J.M (1999). Rheological properties of thermoplastic polyurethane adhesive solutions containing fumed silicas of different surface areas, *International Journal of Adhesion and Adhesives* 19: 321–328.

Keunings, R. (1999). Advances in the computer modeling of the flow of polymeric liquids, *Keynote Lecture, 8th International Symposium on Computational Fluid Dynamics, Bremen, Germany* .

Khan, S. A. & Zoeller, N. J. (1993). Dynamic rheological behaviour of flocculated fumed silica suspensions, *Journal of Rheology* 37(6): 1225–1235.

Kirkwood, K., Kirkwood, J., Wetzel, E. D., Lee, Y. S. & Wagner, N. J. (2004). Yarn pull-out as a mechanism for dissipating ballistic impact energy in kevlar® km-2 fabric - part i: Quasi-static characterization of yarn pull-out, *Textile Research Journal* 74 (10): 920–928.

Landau, L. D. & Lifshitz, E. M. (1987). *Fluid Mechanics*, Pergamon Press, Oxford, Great Britain.

Larson, R. G. (1999). *The Structure and Rheology of Complex Fluids*, Oxford University Press, Nueva York, USA.

Lee, Y. S., Wetzel, E. D. & Wagner, N. J. (2003). The ballistic impact characteristics of kevlar® woven fabrics impregnated with a colloidal shear thickening fluid, *Journal of Materials Science* 38: 2825–2833.

Li, Y., Fedkiw, P. S. & Khan, S. A. (2002). Tithium/v6o13 cells using silica nanoparticled-based composite electrolyte, *Electrochimica Acta* 47: 3853–3861.

Macosko, C. W. (1994). *Rheology: Principles, measurements, and applications*, Wiley-VCH, Inc., USA.

Maranzano, B. J. & Wagner, N. J. (2002). Flow-small angle neutron scattering measurements of colloidal dispersion microstructure evolution through the shear thickening transition, *J. Chem. Phys.* 117(22): 10291–10302.

Masalova, I., Malkin, A. Y., Slatter, P. & Wilson, K. (2003). The rheological characterization and pipeline flow of high concentration water-in-oil emulsions, *Journal of Non-Newtonian Fluid Mechanics* 112: 101–114.

Mezger, T. G. (2002). *The Rheology Handbook: for user of rotational and oscillatory rheometers*, Ed. Vincentz Verlag, Germany.

Morrison, F. A. (2001). *Understanding Rheology*, Oxford University Press, USA.

O'Callaghan, S., Walsh, M. & McGloughlin, T. (2003). Comparison of finite volume, finite element and theoretical predictions of blood flow through an idealised femoral artery, *Summer Bioengineering Conference*, Florida, USA, pp. 417–418.

Ouyang, C., Wang, S., Zhang, Y. & Zhang, Y. (2006). Low-density polyethylene/silica compound modified asphalt with high-temperature storage stability, *Journal of Applied Polymer Science* 101: 472–479.

Papanastasiou, T. C., Georgiou, G. C. & Alexandrou, A. N. (2000). *Viscous fluid flow*, CRC Press LLC, USA.

Phan-Thien, N. (2002). *Understanding Viscoelasticity*, Springer-Verlag Berlin Heidelberg, Germany.

Pinho, F. (2001). The methodology of finite volumes applied to computational rheology. ii-fundamentals for stress-explicit fluids, *Journal of the Portuguese Society of Rheology* 1: 63–100.

Pinho, F. & Oliveira, M. (2001). The methodology of finite volumes applied to computacional rheology: I- introduction, *Journal of the Portuguese Society of Rheology* 1: 1–15.

Raghavan, S. R. & Khan, S. A. (1995). Shear-induced microstructural changes in flocculated suspensions of fumed silica, *Journal of Rheology* 39(6): 1311–1325.

Raghavan, S. R. & Khan, S. A. (1997). Shear-thickening response of fumed silica suspensions under steady and oscillatory shear, *Journal of Colloid and Interface Science* 185: 57–67.

Raghavan, S. R., Walls, H. J. & Khan, S. A. (2000). Rheology of silica dispersions in organic liquids: New evidence of solvations forces dictated by hidrogen bonding, *Langmuir* 16(21): 7920–7930.

Souza-Mendes, P. R. & Dutra, E. S. S. (2004). Viscosity function for yield-stress liquids, *Applied Rheology* 14: 296–302.

Steffe, J. (1996). *Rheological methods in food process engineering*, Ed. Freeman Press, Michigan, USA.

Tanner, R. I. & Walters, K. (1998). *Rheology: An Historical Perspective*, Rheology Series, vol. 7, Ed. Elsevier Science Publishers B.V., Netherlands.

Vermant, J. & Solomon, M. J. (2005). Flow-indiuced structure in colloidal suspensions, *Journal of Physics: Condensed Matter* 17: 187–216.

Walls, H. J., Zhou, J., Yerian, J. A., Fedkiw, P. S., Khan, S. A., Stowe, M. K. & Baker, B. L. (2000). Fumed-silica based composite polymer electrolyte: synthesis, rheology and electrochemistry, *Journal of Power Sources* 89: 156–162.

Walters, K. (1975). *Rheometry*, Chapman and Hall Ltd., London, Great Britain.

Wesseling, P. (2001). *Principles of computational fluid dynamics*, Ed. Springer Verlag, Berlin, Germany.

Yziquel, F., Carreau, P. J. & Tanguy, P. A. (1999). Non-linear viscoelastic behavior of fumed silica suspensions, *Rheologica Acta* 34: 14–25.

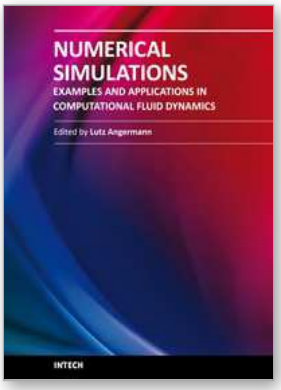

Numerical Simulations - Examples and Applications in Computational Fluid Dynamics

Edited by Prof. Lutz Angermann

ISBN 978-953-307-153-4
Hard cover, 440 pages
Publisher InTech
Published online 30, November, 2010
Published in print edition November, 2010

This book will interest researchers, scientists, engineers and graduate students in many disciplines, who make use of mathematical modeling and computer simulation. Although it represents only a small sample of the research activity on numerical simulations, the book will certainly serve as a valuable tool for researchers interested in getting involved in this multidisciplinary ï¬eld. It will be useful to encourage further experimental and theoretical researches in the above mentioned areas of numerical simulation.

How to reference

In order to correctly reference this scholarly work, feel free to copy and paste the following:

F.j. Galindo-rosales and F.j. Rubio-hernández (2010). Numerical Simulation in Steady Flow of Non-Newtonian Fluids in Pipes with Circular Cross-Section, Numerical Simulations - Examples and Applications in Computational Fluid Dynamics, Prof. Lutz Angermann (Ed.), ISBN: 978-953-307-153-4, InTech, Available from: http://www.intechopen.com/books/numerical-simulations-examples-and-applications-in-computational-fluid-dynamics/numerical-simulation-in-steady-flow-of-non-newtonian-fluids-in-pipes-with-circular-cross-section

INTECH
open science | open minds

InTech Europe
University Campus STeP Ri
Slavka Krautzeka 83/A
51000 Rijeka, Croatia
Phone: +385 (51) 770 447
Fax: +385 (51) 686 166
www.intechopen.com

InTech China
Unit 405, Office Block, Hotel Equatorial Shanghai
No.65, Yan An Road (West), Shanghai, 200040, China
中国上海市延安西路65号上海国际贵都大饭店办公楼405单元
Phone: +86-21-62489820
Fax: +86-21-62489821